lubricants

MDPI

Article

Static Characteristics of a Micro Bidirectional Rotating Thrust Bearing with Novel Herringbone Grooves

Tianming Ren * and Ming Feng

School of Mechanical Engineering, University of Science and Technology Beijing, Beijing 100083, China
* Correspondence: rentianming@ustb.edu.cn

Abstract: Bidirectional rotating thrust bearings are critical components for the development of bidirectional equipment. This paper presents the design and numerical study of an oil-lubricated bidirectional rotating thrust bearing with novel herringbone grooves, which consists of three groups of spiral grooves. The lubrication mechanism of the novel herringbone grooves is revealed. The static characteristics of the thrust bearing are numerically investigated by solving the Reynolds equation applying the finite element method. The influences of the radial width, depth, angle, circumferential width ratio, and number of the groove on the bearing performance are analyzed. The results show that there exists an optimal combination of groove radial widths that ensures equal load capacities in both rotation directions while achieving their maximum values. Furthermore, optimal values for the depth, angle, circumferential width ratio, number of the grooves can also enhance the bearing's load capacity, maximum film pressure, and energy efficiency. Additionally, it is found that groove radial width has the most significant influence on the bearing performance difference under different rotation directions, followed by the effects from the angle, number, circumferential width ratio, and depth of the groove. The conclusions obtained can provide a valuable reference for the research and application of bidirectional thrust bearings.

Keywords: bidirectional rotating thrust bearings; herringbone groove; bearing performance

check for updates

Received: 13 February 2025
Revised: 27 February 2025
Accepted: 1 March 2025
Published: 2 March 2025

Citation: Ren, T.; Feng, M. Static Characteristics of a Micro Bidirectional Rotating Thrust Bearing with Novel Herringbone Grooves. *Lubricants* **2025**, *13*, 109. https://doi.org/10.3390/lubricants13030109

Copyright: © 2025 by the authors. Licensee MDPI, Basel, Switzerland. This article is an open access article distributed under the terms and conditions of the Creative Commons Attribution (CC BY) license (https://creativecommons.org/licenses/by/4.0/).

1. Introduction

With the rapid advancement of technology and increasing industrial demands, there has been a significant rise in the requirement for bidirectional rotating equipment, such as tape drives [1], robot joints [2], and reaction kettles [3]. Bearings are one of the key components of this industrial equipment, significantly influencing their performance and reliability. Compared to rolling element bearings, fluid film bearings have the advantage of compact structure, low friction, low noise, long service life, and high shock resistance, making them widely utilized in modern electronic devices, such as machine tool spindles [4], turbomachinery [5,6], and hard disk drives [7]. To enhance key performance metrics such as load capacity and stability, fluid film bearings are usually designed with various grooves such as spiral groove [8,9], stepped groove [10,11], and herringbone groove [12,13]. However, these grooves typically exhibit unidirectionality, which restricts fluid film bearings to rotate primarily in a designated direction. Rotation in the opposite direction results in a notable decline in bearing performance.

To broaden the application of fluid film bearings, research on bidirectional rotating fluid film bearings is progressively gaining more attention. Kawabata [14] proposed a bidirectional rotating herringbone-grooved journal bearing. Compared with the common

herringbone groove structure, this groove type has an additional set of spiral grooves. The study showed that the load capacity and the radial load component of the proposed bearing do not differ greatly from those of traditional bearings. Wu [15] conducted a stability analysis on the bidirectional rotating journal bearing with similar grooves under different design parameters. The findings indicated that the bearing capacity and stability in the forward rotation are marginally lower than those of unidirectional herringbone groove bearings, while the performance in the reverse rotation is superior. Zhang [16] proposed a bidirectional rotating fluid bearing system and investigated its power consumption. The results demonstrated that, for the same load capacity and stiffness requirement, the power consumption of a bidirectional rotating fluid bearing system is about 50% higher than that of a unidirectional rotating fluid film bearing system, assuming both bearing systems have the same dimensions. To improve the bearing performance, Chen [17] carried out an optimized design of the bidirectional rotating herringbone journal bearing by considering the cavity boundary problem, and the results showed that the optimum groove parameters, which enable a maximum load capacity and a minimum side leakage, can be efficiently obtained.

The above studies provide valuable references for the design and application of bidirectional rotating fluid film bearings. However, most of these studies focus on journal bearings, while research on bidirectional rotating thrust bearings remains relatively scarce. Tilting pad thrust bearings can rotate clockwise and counterclockwise when centrally supported, and spring support structures can be used to increase the load capacity [18]. However, due to their complex structure, such bearings are primarily suitable for large-scale equipment. In Zhang's [16] design of a bidirectional rotating fluid bearing system, regular herringbone grooves bounded by two flat regions at the inner and outer edges of the thrust plate were utilized in the thrust bearing. It was found that, for the same diameter, the load capacity of the bidirectional rotating thrust bearing is much lower than that of the unidirectional rotating thrust bearings.

The above research shows that although the performance of the bidirectional bearing is slightly inferior to that of the unidirectional bearing, it provides an important advantage of bidirectional rotation for the system and significantly expands the application range of the fluid film bearing. This paper proposes a micro bidirectional rotating bearing designed specifically for micro fans with a diameter of 4 mm. The reduction in size, combined with the requirement for bidirectional rotation, leads to a decreased load capacity of the thrust bearing, thereby raising concerns regarding its overall performance. Consequently, this study introduces a design featuring novel herringbone grooves. Following an examination of the lubrication mechanism associated with these novel herringbone grooves, a numerical investigation is conducted to assess the static characteristics of the bearing, including load capacity, pressure distribution, and friction torque. The influences of the radial width, depth, angle, circumferential width ratio, and number of the groove on the bearing performance are analyzed.

2. Model and Equations

2.1. Bearing Configuration

Figure 1 shows the configuration of the bidirectional rotating thrust bearing with novel herringbone grooves. The grooves are designed on a stationary sleeve, while the rotating shaft has a smooth surface. Three groups of spiral grooves are radially arranged on the sleeve surface, with widths denoted as B_1, B_2, and B_3, respectively. The groove angles of these three groups of grooves are equal in magnitude; however, the direction of the angle for the middle group of grooves is opposite to that of the inner and outer groups. Additionally, all three groups of grooves share identical depths, width ratios, and numbers. This arrangement forms an overall 'Z-type' structure, enabling the bearing to support

bidirectional rotation. When the smooth shaft rotates in a clockwise direction, the middle and outer groups of spiral grooves pump lubricating oil into the bearing, generating oil film pressure and load capacity. Conversely, when the shaft rotates in a counterclockwise direction, the inner and outer groups of spiral grooves perform this function.

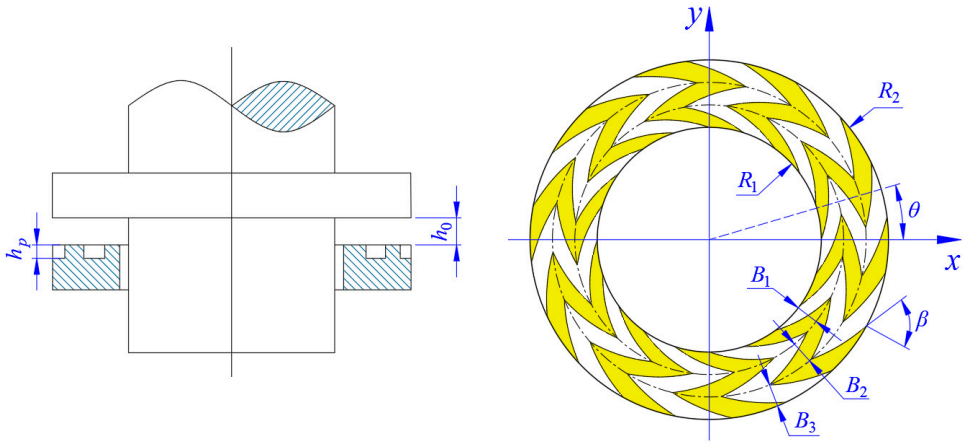


Figure 1. Configuration of the bidirectional rotating thrust bearing.

2.2. Governing Equations

2.2.1. Reynolds Equation

According to the properties of the lubricated oil and the operation condition of the thrust bearing, some assumptions are made as follow:

(1) The thickness of the oil film is far smaller than the radius and width of the bearing, and the curvature of the oil film can be neglected.
(2) The pressure of the oil film in the thickness direction is constant.
(3) Only the velocity gradient in the film thickness direction is considered.
(4) The lubricating oil is assumed to be in an isothermal state.
(5) The oil-lubricated bearings work under no-slip velocity boundary conditions.

The Reynolds equation describing the oil film pressure in the thrust bearing is written as follows:

$$\frac{\partial}{\partial\theta}\left(\frac{h^3}{\mu}\frac{\partial P}{\partial\theta}\right)+r\frac{\partial}{\partial r}\left(\frac{rh^3}{\mu}\frac{\partial P}{\partial r}\right)=6\omega r^2\frac{\partial h}{\partial\theta} \tag{1}$$

where θ and r are the circumferential and radius coordinates of the thrust bearing, P is the oil film pressure, ω is the bearing rotation speed, μ is the viscosity of lubricating oil, and h is the thickness of the oil film, which is defined by:

$$h = h_0 + \Delta h_p \tag{2}$$

where h_0 is the bearing clearance and h_p is the groove depth (Δ = 1 for the film in the groove; Δ = 0 for the rest).

2.2.2. Boundary Conditions

The film pressures at the inner and outer sides of the thrust bearing are equal to the ambient pressure:

$$P(\theta, R_1) = P(\theta, R_2) = 0bar \tag{3}$$

In the study of fluid film bearings, internal boundary conditions are also employed to describe the cavitation pressure of the oil film. The Reynolds boundary conditions, which consider pressure continuity and flow conservation, are used in this paper:

$$P(\theta, r) = 0, \text{ if } P(\theta, r) < 0 \tag{4}$$

$$\frac{\partial P}{\partial \theta} = 0 \text{ at } \theta = \theta^* \tag{5}$$

where θ^* is the starting position of the cavitated area.

2.2.3. Load Capacity and Friction Torque

The bearing load capacity along the axial direction and the friction torque around the rotation direction can be calculated by the integration of the pressure of the oil film:

$$F = \int_{R_1}^{R_2} \int_{0}^{2\pi} P r d\theta dr \tag{6}$$

$$M_z = \int_{R_1}^{R_2} \int_{0}^{2\pi} \left(\frac{h}{2} \frac{\partial P}{\partial \theta} + \frac{\mu \omega r}{h} \right) r d\theta dr \tag{7}$$

3. Numerical Algorithms and Verification

3.1. Numerical Algorithm

A program is developed for the calculation of the oil-lubricated thrust bearing, as shown in Figure 2. The film thickness (Equation (2)) is first calculated with the given bearing geometrical and operating parameters. Then, based on the finite element method, the oil film pressure is obtained by solving the Reynolds equation (Equation (1)) and boundary conditions (Equations (3)–(5)). The iteration continues until the oil film reaches convergence accuracy δ, which is defined by:

$$\delta = \left| \frac{P(\theta, r)^i - P(\theta, r)^{i-1}}{P(\theta, r)^{i-1}} \right| \tag{8}$$

where the convergence accuracy is given as 10^{-4} in this study. Finally, the load capacity and friction torque of the thrust bearing are calculated by Equations (6) and (7).

3.2. Verification

Given the absence of both theoretical and experimental research on the thrust bearings with novel herringbone grooves, this study validates the present model through a comparison with the results on the conventional herringbone groove bearings in the literature [19]. Figure 3 shows the comparison of the load capacities of the thrust bearing under various rotation speeds. As it can be seen, the results of the presented model are in good agreement with those presented in the literature. Thus, the correctness of the mathematical model and the accuracy of the numerical algorithm can be verified.

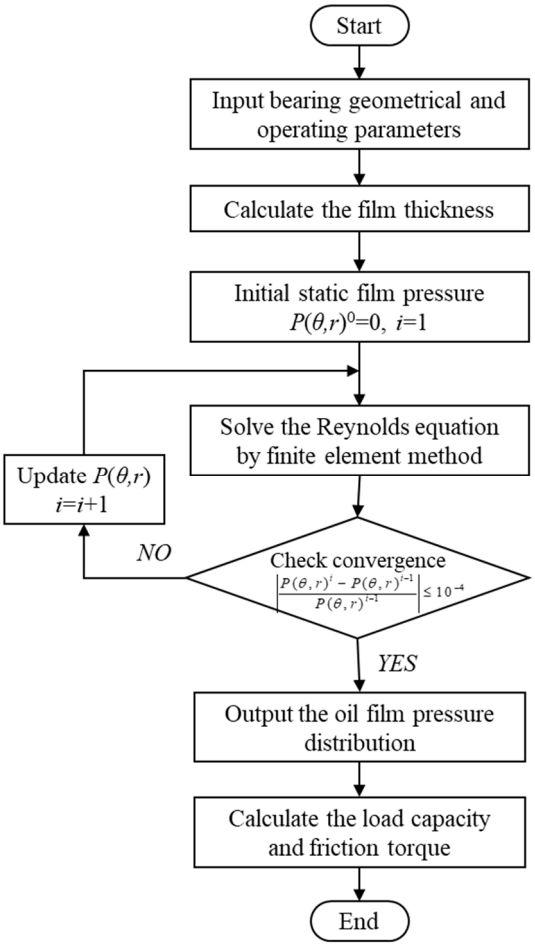


Figure 2. Flow chart.

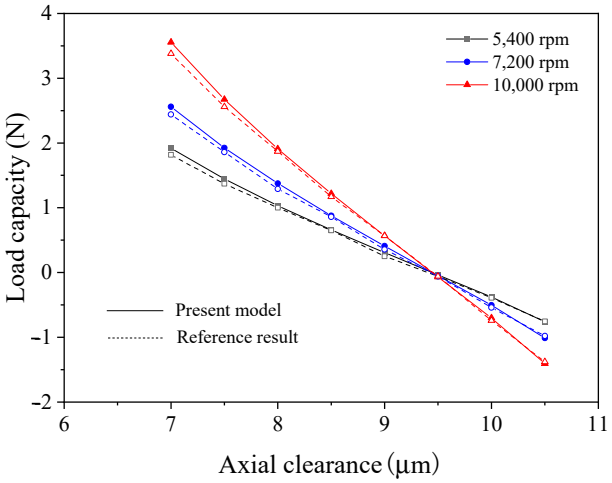


Figure 3. Comparison of the results of the present model with those in the literature.

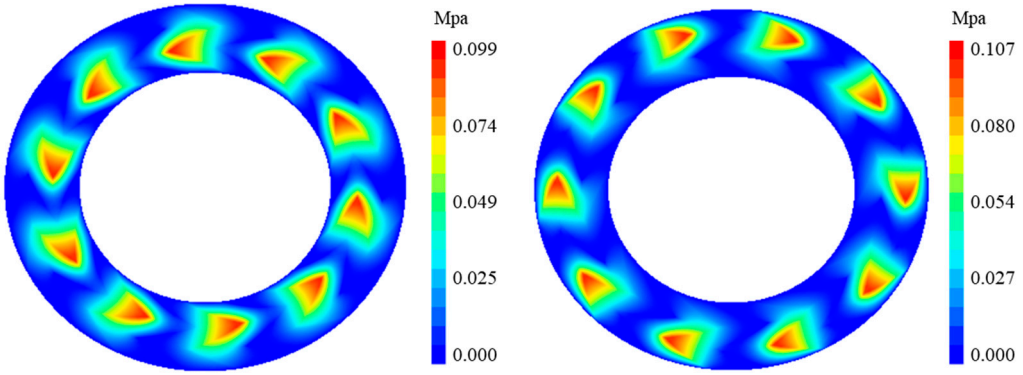
4. Results and Discussion

The parameters of the oil-lubricated bidirectional rotating thrust bearing used in the following study are given in Table 1. The load capacity, maximum film pressure, friction torque, and energy efficiency (the ratio between load capacity and friction torque) of the thrust bearing are analyzed, the effects of parameters including the radial width, depth, angle, circumferential width ratio, and number of the herringbone grooves are theoretically investigated.

Table 1. The parameters of the bidirectional rotating thrust bearing.

Parameter	Value
Bearing inner radius R_1/mm	2.5
Bearing outer radius R_2/mm	4.0
Bearing clearance h_0/μm	5.0
Groove number N	10
Groove radial width B_1/mm	0.53
Groove radial width B_2/mm	0.50
Groove radial width B_3/mm	0.47
Groove angle β/°	55
Groove depth h_p/μm	6
Groove circumferential width ratio	0.45
Oil density ρ/g·cm^{-3}	9.23
Oil viscosity μ/Pa·s	0.018

Figure 4 shows the typical film pressure distributions of the thrust bearing under different rotation directions. As shown in Figure 4a, when the bearing rotates counterclockwise, the high-pressure region of the oil film is predominantly located at the inner side. This pressure is primarily generated by the pumping effect of the two inner spiral grooves, with the peak oil film pressure occurring at the interface between the inner and middle spiral grooves. Conversely, when the bearing rotates clockwise, the oil film pressure is mainly produced by the pumping effect of the two outer spiral grooves, shifting the high-pressure region towards the outer side, with the maximum pressure observed at the boundary between the middle and outer spiral grooves. This pressure distribution aligns with the design objectives of the novel herringbone groove.



(**a**) (**b**)

Figure 4. Pressure distributions of the bidirectional thrust bearing under different rotating directions: (**a**) counterclockwise; (**b**) clockwise.

4.1. Influence of Groove Radial Width

Figure 5 shows the variation in bearing load capacity with groove radial width under different clearances. In the calculation, the rotation speed is 1000 rpm. As it can be seen, the increment in the inner groove width B_1 leads to a rise in the bearing load capacity when rotating counterclockwise, whereas the bearing load capacity, when rotating clockwise, decreases. This phenomenon can be attributed to the inverse relationship between B_1 and B_3. As B_1 increases, B_3 decreases, thereby enhancing the dynamic effect of the two inner spiral grooves while simultaneously diminishing the dynamic effect of the outer ones. Additionally, when B_1 remains constant, the increment in the middle groove width B_2 results in an increase in the load capacity along the counterclockwise direction, whereas the load capacity along the counterclockwise direction is correspondingly reduced.

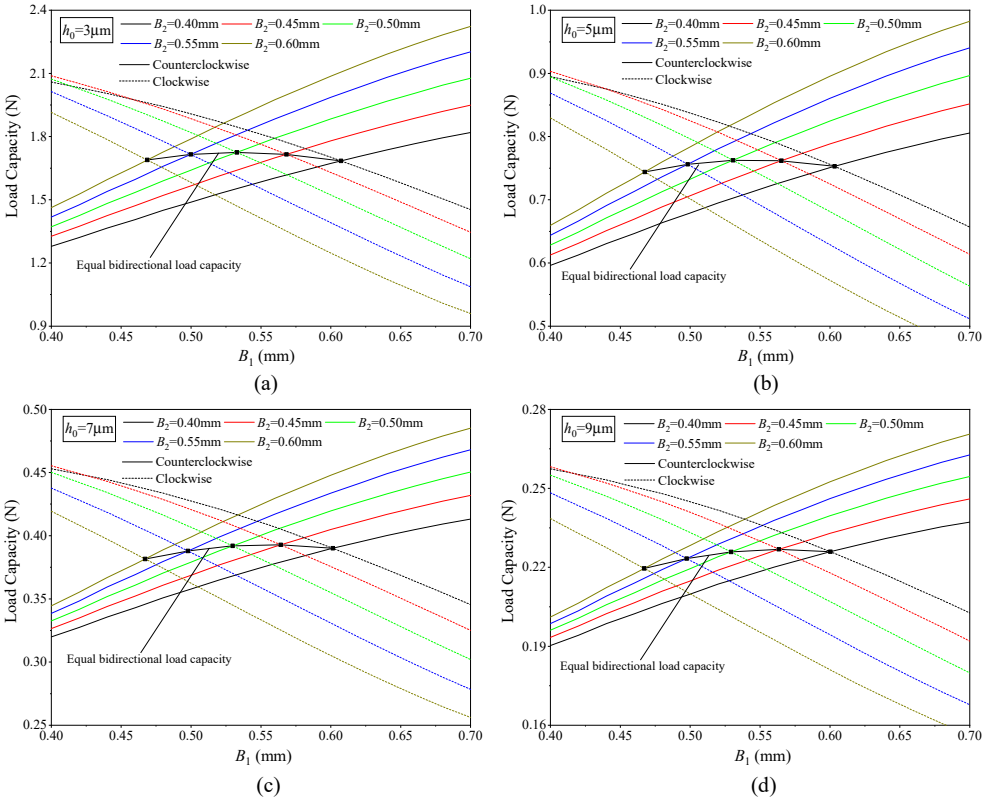


Figure 5. Variation in bearing load capacity with groove radial width: (**a**) h_0 = 3 μm; (**b**) h_0 = 5 μm; (**c**) h_0 = 7 μm; (**d**) h_0 = 9 μm.

In bidirectional rotating mechanical equipment, it is crucial to ensure that the bearings exhibit the same performance during both counterclockwise and clockwise rotations in order to achieve stable system operation. The intersection points of load capacities along the two different directions represent the position where the bidirectional bearing load capacity is identical. At this juncture, the width parameter of the herringbone groove ensures that the thrust bearing exhibits the same characteristics during rotation in both directions. The curve of the equal bidirectional load capacity of the thrust bearing is also given in Figure 5. As it can be seen, with the increase in B_1, the bidirectional load capacity of the thrust bearing shows a trend of first increasing and then decreasing. The maximum bidirectional load capacity can be obtained when B_1 = 0.53 mm and B_2 = 0.50 mm.

It can be observed from the figure that, as the bearing clearance increases, the bearing load capacity decreases. However, the influence of the groove radial width on the bearing load capacity remains constant.

Figure 6 shows the variations in the maximum film pressure and the friction torque of the thrust bearing with groove radial width. In the calculation, the bearing clearance is 5 μm, while the groove widths are B_1 = 0.53 mm, B_2 = 0.50 mm, and B_3 = 0.47 mm. As it can be seen, the bearing load capacity exhibits a slight decrease as B_2 increases, whereas the variation in the thrust bearing friction torque remains relatively minor. Additionally, the maximum film pressure and friction torque are both higher during clockwise rotation compared to during counterclockwise rotation. This is primarily due to the fact that, during clockwise rotation, the maximum film pressure occurs at the boundary between the middle and outer grooves, where the radius is larger than that of the corresponding boundary during counterclockwise rotation. Consequently, the dynamic effect is more pronounced, resulting in higher oil film pressure.

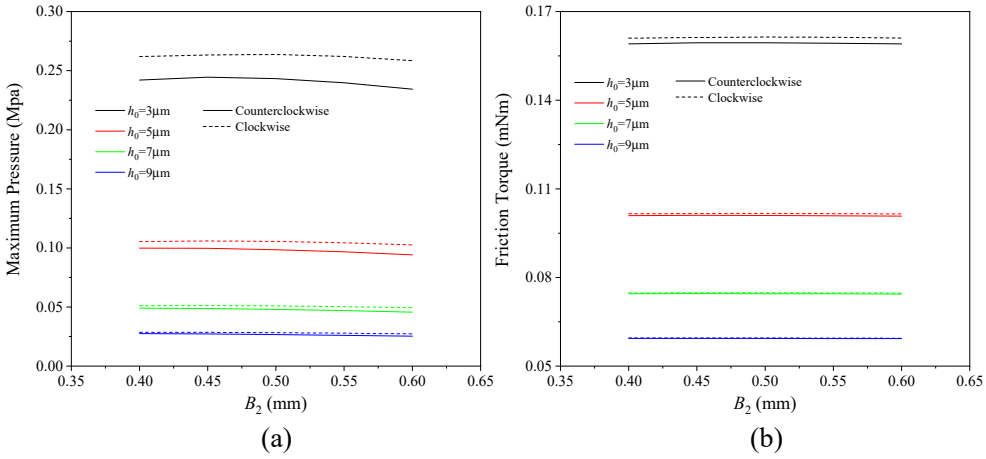


Figure 6. Variation in bearing maximum film pressure and friction torque with groove radial width: (**a**) maximum pressure; (**b**) friction torque.

4.2. Influence of Groove Depth

Figure 7 shows the variations in bearing static characteristics with groove depth under different clearances. As it can be seen in Figure 7a, with the increment of the groove depth d_p, the load capacity of the thrust bearing first increases and then decreases, indicating that there exists an optimal groove depth to maximize the load capacity. The optimal groove depths are 3 μm, 5 μm, 7 μm, and 9 μm, respectively, when the bearing clearances are 3 μm, 5 μm, 7 μm, and 9 μm. The optimal groove depth increases with the increase in the clearance, yet the ratio h_p/h_0 remains constant at 1. The maximum film pressure and the bearing energy efficiency exhibit a similar trend to the load capacity, as shown in Figure 7b,d. However, in Figure 7c, the bearing friction torque increases with the increase in clearance, and this changing trend is not affected by the clearance.

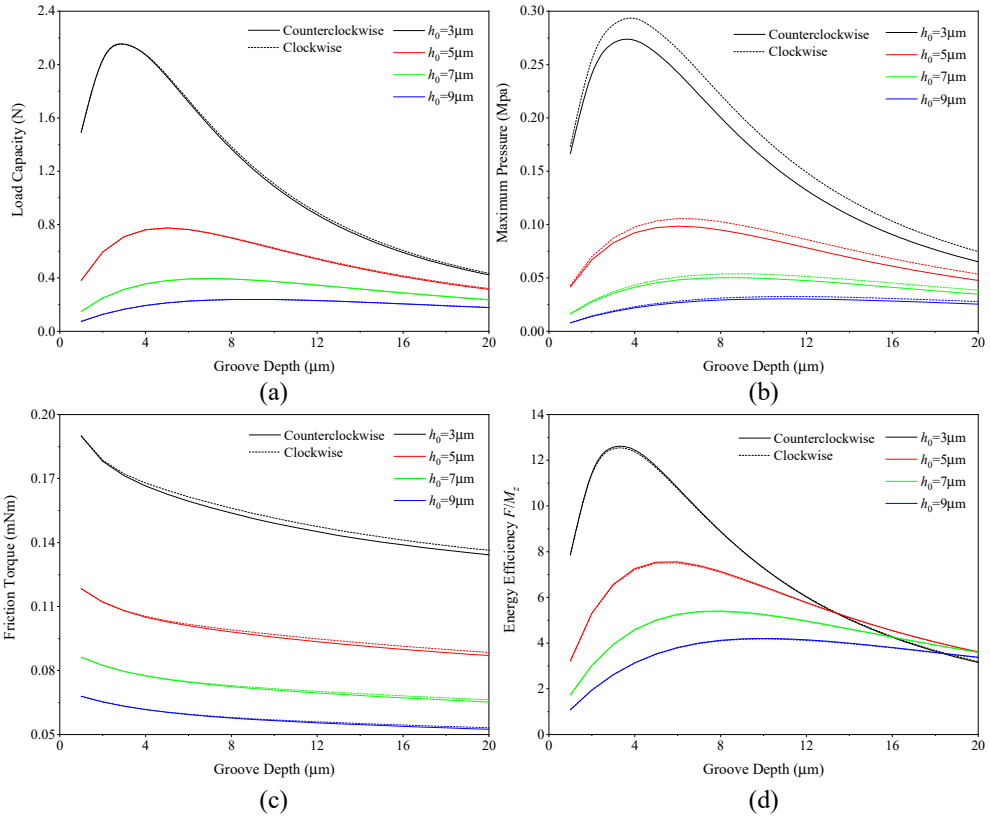


Figure 7. Variation in bearing static characteristics with groove depth: (**a**) load capacity; (**b**) maximum pressure; (**c**) friction torque; (**d**) energy efficiency.

Furthermore, the load capacity and energy efficiency of the bearing in anticlockwise rotation and clockwise rotation are almost the same, indicating that the groove depth does not affect the difference in bearing performance under different rotation directions.

4.3. Influence of Groove Angle

Figure 8 shows the variations in bearing static characteristics with groove angle under different clearances. As it can be seen, the bearing load capacity, maximum film pressure, and energy efficiency ratio exhibit the same variation trend. Their values all first increase and then decrease with the increment of groove angle. The optimal groove angles are 68°, 55°, 44°, and 31°, respectively, when the bearing clearances are 3 μm, 5 μm, 7 μm, and 9 μm. The optimal groove angle decreases with the increase in the bearing clearance. The research results show that the selection of the optimal groove angle is closely related to the bearing operating clearance or external load. Large groove angles are suitable for applications with small operating clearances or high external loads, while small groove angles are appropriate for conditions with large operating clearances or small external loads. It should be pointed out that with the increase in the bearing clearance, the influence of the groove angle on the load capacity gradually weakens. However, the influence of the groove angle on the friction torque is relatively small. When the groove angle varies within the range of 20° to 60°, the friction torque remains almost unchanged. Within the range of 20° to 60°, variations in the groove angle have little effect on the friction torque, which remains nearly constant. For groove angles exceeding 60°, the friction torque exhibits a slight decrease as the groove angle increases.

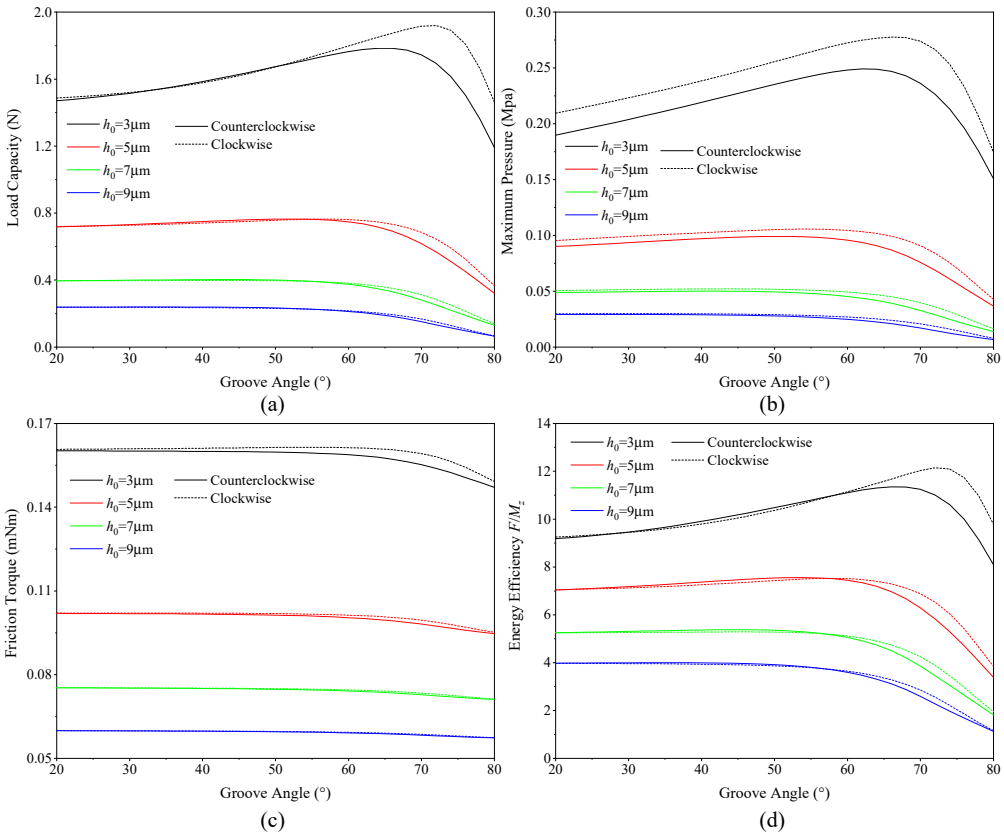


Figure 8. Variation in bearing static characteristics with groove angle: (**a**) load capacity; (**b**) maximum pressure; (**c**) friction torque; (**d**) energy efficiency.

Furthermore, it can also be seen that when the groove angle is less than 50°, the bearing load capacities, when rotating counterclockwise, are almost the same as these when rotating clockwise. When the groove angle is greater than 60°, the bearing load capacities during

clockwise rotation are greater than those during counterclockwise rotation. The results show that, as the groove angle is greater than 60°, the bearing performance differences under different rotation directions will increase.

4.4. Influence of the Groove Circumferential Width Ratio

Figure 9 shows the variations in bearing static characteristics with the groove circumferential width ratio under different clearances. As it can be seen, with the increase in the groove circumferential width ratio, the load capacity, maximum film pressure, and energy efficiency showed a trend of first increasing and then decreasing. The optimal groove circumferential width ratio with the maximum load capacity is 0.45 and does not change with the bearing clearance, while the optimal value for the maximum energy efficiency is about 0.6. Meanwhile, the friction torque decreases as the groove circumferential width ratio increases.

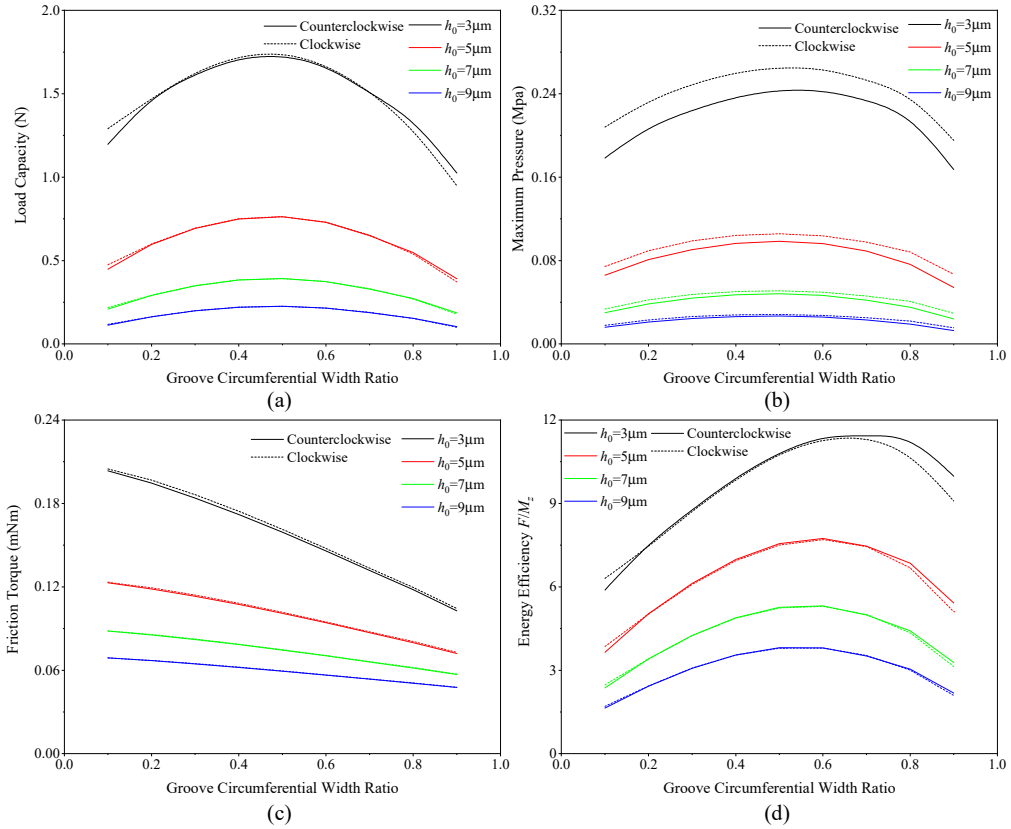


Figure 9. Variation in bearing static characteristics with the groove circumferential width ratio: (**a**) load capacity; (**b**) maximum pressure; (**c**) friction torque; (**d**) energy efficiency.

In addition, it can also be seen that when the circumferential width ratio is less than 0.7, the bearing load capacities when rotating counterclockwise are larger than that when rotating clockwise. When the groove circumferential width ratio is larger than 0.7, the bearing load capacities during clockwise rotation are smaller than these during counterclockwise rotation. However, it should be pointed out that the influence of the groove circumferential width ratio on the bearing performance differences under different rotation directions is relatively small.

4.5. Influence of the Groove Number

Figure 10 shows the variations in bearing static characteristics with the groove number under different clearances. As shown in Figure 10a, the bearing load capacity initially increases and then slightly decreases with the increasing groove number. The load capacities,

when rotating counterclockwise, reaches their peak when the groove number is 9, whereas the load capacities when rotating clockwise peak at 11 grooves. When the groove number exceeds 10, the influence of the groove number on load capacity becomes negligible. As the groove number increases, there is a slight decrease in the maximum film pressure, while the friction torque exhibits a slight increase, as shown in Figure 10b,c. As for the energy efficiency, its variation trend with the groove number is the same as that of load capacity, as shown in Figure 10d.

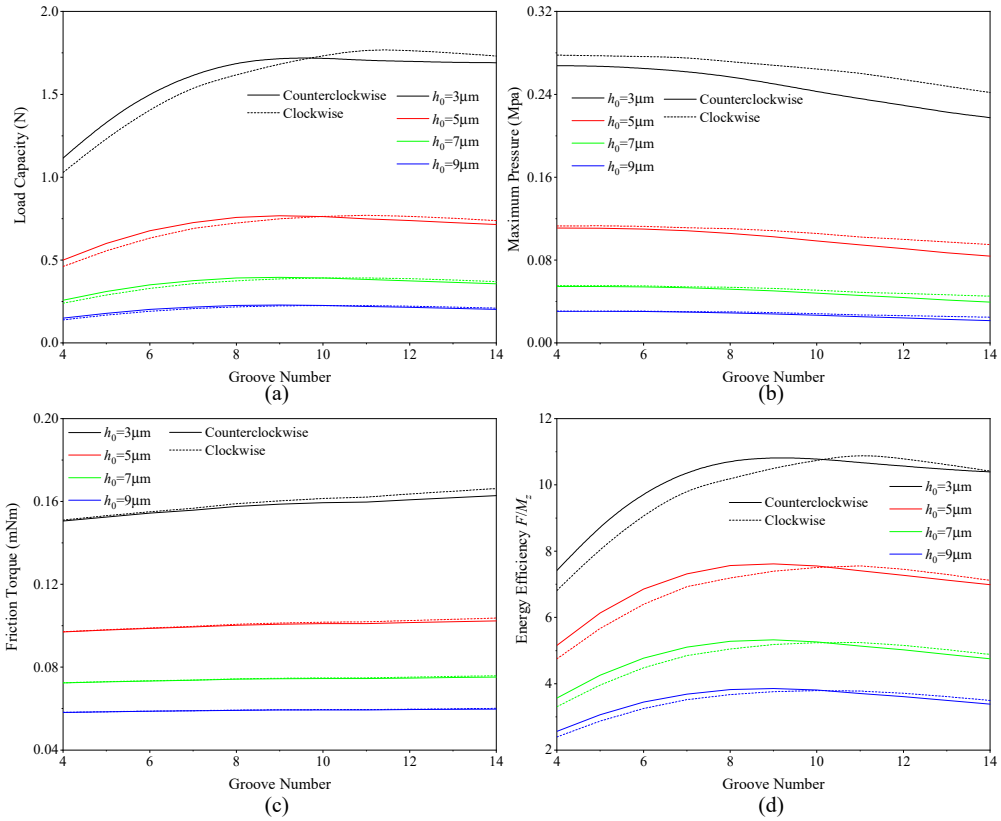


Figure 10. Variation in bearing static characteristics with the groove number: (**a**) load capacity; (**b**) maximum pressure; (**c**) friction torque; (**d**) energy efficiency.

Moreover, when the groove number is fewer than 10, the load capacity and energy efficiency of the bearing when rotating counterclockwise are superior to those observed in clockwise rotation. Conversely, when the groove number is larger than 10, both the load capacity and energy efficiency when rotating counterclockwise are lower than those when rotating clockwise.

4.6. Influence of Rotation Speed

Figure 11 shows the variations in bearing static characteristics with rotation speed under different clearances. As it can be seen, the bearing load capacity, maximum film pressure, and friction torque increase linearly with rotation speed. However, the energy efficiency is almost unaffected by rotation speed. Moreover, at different rotational speeds, the load capacity and energy efficiency of bearings when rotating counterclockwise are nearly equivalent to those of bearings when rotating clockwise, indicating that the rotation speed has little influence on the difference between the two directions.

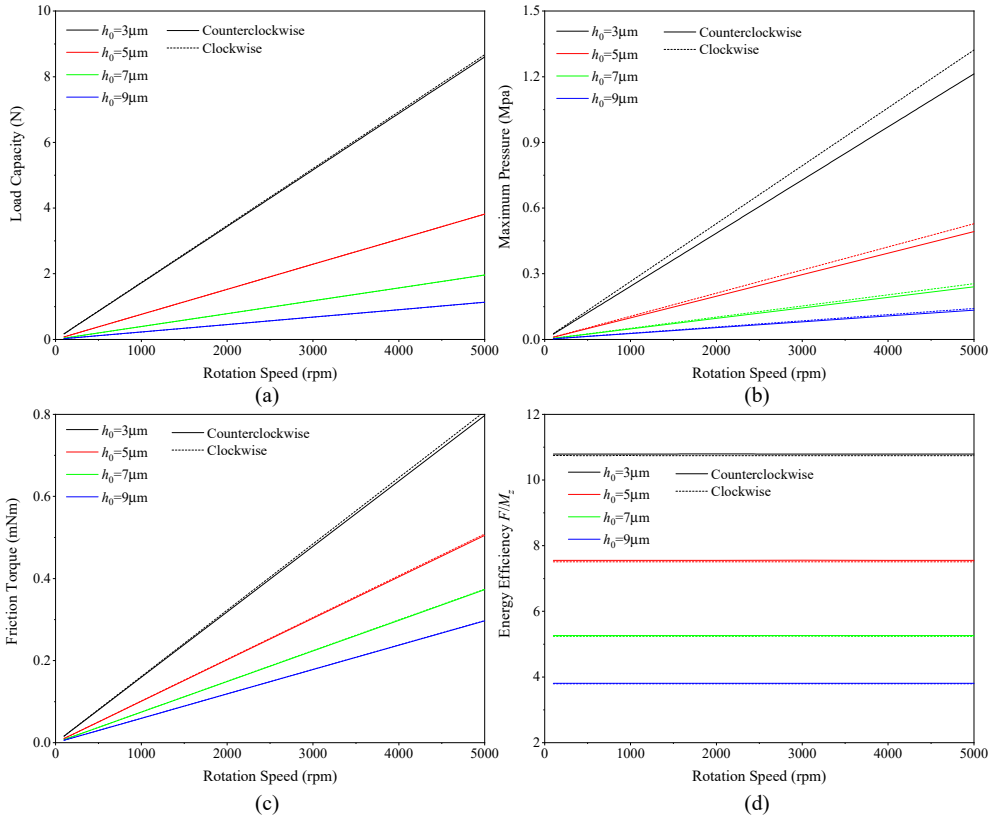


Figure 11. Variation in bearing static characteristics with rotation speed: (**a**) load capacity; (**b**) maximum pressure; (**c**) friction torque; (**d**) energy efficiency.

5. Conclusions

This paper proposed a novel herringbone groove configuration consisting of three groups of spiral grooves designed for bidirectional rotating thrust bearing. When the bearing rotates counterclockwise, the dynamic pressure of the lubricating oil generated by the inner and middle groups of spiral grooves contributes to its load capacity; conversely, when it rotates clockwise, the dynamic pressure from the middle and outer groups of spiral grooves provides this capacity. A lubrication model was developed to numerically analyze various static characteristics, including the bearing load capacity, maximum film pressure, friction torque, and energy efficiency. The following conclusions were drawn:

(1) There exists a group of groove radial widths at which the bidirectional load capacity is equal, and the bidirectional load capacity first increases and then decreases with the increase in B_2. The optimal combination of groove radial widths are B_1 = 0.53 mm, B_2 = 0.50 mm, and B_3 = 0.47 mm.

(2) There exist optimal values for the depth, angle, width ratio, and number of the grooves that can maximize the bearing's load capacity, maximum film pressure, and energy efficiency.

(3) With the increment of rotation speed, the bearing load capacity, maximum film pressure, and friction torque increase linearly, while the energy efficiency remains unchanged.

(4) The groove radial width has the most significant influence on the performance difference under different rotation directions, followed by the groove angle, groove number, and circumferential width ratio of the groove. In contrast, groove depth and rotation speed have the least influence.

Author Contributions: Conceptualization, T.R. and M.F.; methodology, T.R. and M.F.; software, T.R.; validation, T.R. and M.F.; formal analysis, T.R.; investigation, T.R. and M.F.; resources, M.F.; data

curation, T.R.; writing—original draft preparation, T.R.; writing—review and editing, T.R. and M.F.; visualization, T.R. and M.F.; supervision, M.F.; project administration, T.R.; funding acquisition, T.R. and M.F. All authors have read and agreed to the published version of the manuscript.

Funding: This research was funded by the National Key Research and Development Program of China (grant number: 2022YFB3402701).

Data Availability Statement: The data presented in this study are available on reasonable request from the corresponding author.

Conflicts of Interest: The authors declare no conflict of interest.

References

1. Lantz, M.A.; Furrer, S.; Petermann, M.; Rothuizen, H.; Brach, S.; Kronig, L.; Iliadis, I.; Weiss, B.; Childers, E.R.; Pease, D. Magnetic Tape Storage Technology. *ACM Trans. Storage* **2025**, *21*, 1–70. [CrossRef]
2. Xia, B.; Wang, K.; Xu, A.; Zeng, P.; Yang, N.; Li, B. Intelligent Fault Diagnosis for Bearings of Industrial Robot Joints Under Varying Working Conditions Based on Deep Adversarial Domain Adaptation. *IEEE Trans. Instrum. Meas.* **2022**, *71*, 3508313. [CrossRef]
3. Liu, Q.; Wang, S.; Xu, J.; Sun, H.; Wang, H. Enhanced Particle Mixing Performance of Liquid-Solid Reactor under Non-Periodic Chaotic Stirring. *Chem. Eng. Res. Des.* **2024**, *211*, 78–94. [CrossRef]
4. Sun, Z.; Guan, C.; Xu, H.; Hu, H.; Dai, Y. The Influence of Journal's Roundness on Rotating Accuracy of Aerostatic Spindle and Precision Improvement by Time-Controlled Grinding. *Tribol. Int.* **2024**, *197*, 109805. [CrossRef]
5. Ren, T.; Feng, M. Theoretical and Experimental Study on the Stability of Water Lubricated High Speed Journal Bearing with Lobe Pockets. *Tribol. Int.* **2023**, *187*, 108665. [CrossRef]
6. Han, D.; Bi, C. The Partial Derivative Method for Dynamic Stiffness and Damping Coefficients of Supercritical CO2 Foil Bearings. *Lubricants* **2022**, *10*, 307. [CrossRef]
7. Wang, J.; Ran, H.; Dai, P.; Yan, S.; Yao, X.; Wang, F.; Zuo, G. Flow Characteristic Analysis of a Herringbone Groove Thrust Bearing with Shaft Misalignment. *Ind. Lubr. Tribol.* **2023**, *75*, 67–73. [CrossRef]
8. Song, L.; Yuan, G.; Zhang, H.; Ding, Y.; Cheng, K. The Stability of Spiral-Grooved Air Journal Bearings in Ultrahigh Speeds. *Materials* **2022**, *15*, 1759. [CrossRef]
9. Lin, X.; Wang, S.; Jiang, S.; Zhang, S. Dynamic Characteristics of High-Speed Water-Lubricated Spiral Groove Thrust Bearing Based on Turbulent Cavitating Flow Lubrication Model. *Chin. J. Mech. Eng.* **2022**, *35*, 13. [CrossRef]
10. Wang, L.; Pei, S.; Xiong, X.; Xu, H. Study on the Static Performance and Stability of a Water-Lubricated Hybrid Bearing with Circumferential Grooves and Stepped Recesses Considering the Influence of Recess Sizes. *Tribol. Trans.* **2014**, *57*, 36–45. [CrossRef]
11. Wang, L.; Xu, H. Experimental Study on the Dynamic Performance of a New High-Speed Spindle Supported by Water-Lubricated Hybrid Bearings. *Shock Vib.* **2016**, *2016*, 8297834. [CrossRef]
12. Ran, H.; Dai, P.; Yan, S.; Wang, F.; Yao, X.; Wang, J.; Zuo, G. Flow Mechanisms and Lubrication Performance of Water-Lubricated Thrust Bearings with Herringbone Grooves. *Lubricants* **2022**, *10*, 182. [CrossRef]
13. Liu, W.; Gjika, K.; Schiffmann, J. Design and Experimental Investigation of a Herringbone Grooved Gas Bearing Supported Turbocharger. *Mech. Syst. Signal Process.* **2023**, *186*, 109828. [CrossRef]
14. Kawabata, N.; Ozawa, Y.; Kamaya, S.; Miyake, Y. Static Characteristics of the Regular and Reversible Rotation Type Herringbone Grooved Journal Bearing. *J. Tribol.* **1989**, *111*, 484–490. [CrossRef]
15. Wu, J.K.; Li, A.F. Dynamical Performance of Two-Way Herringbone Grooved Liquid-Lubricated Journal Bearing. *Mech. Sci. Technol. Aerosp. Eng.* **2002**, *21*, 228–230. (In Chinese)
16. Zhang, Q.D.; Chen, S.X.; Yang, J.P.; Winoto, S.H. A Bi-Directional Rotating Fluid Bearing System. *Microsyst. Technol.* **2002**, *8*, 271–277. [CrossRef]
17. Chen, C.-Y.; Liu, C.-S.; Tee, C.-K.; Li, Y.-C. Application of Stabilized Term in Free Boundary Problems for Optimizing Bi-Directional-Rotation Herringbone-Grooved Journal Bearings. *Appl. Math. Model.* **2017**, *47*, 826–838. [CrossRef]
18. Yang, S.; Zheng, W.; Jiang, M.; Pei, S.; Xu, H. A Comparative Experimental Study on Large Size Center and Bi-Directional Offset Spring-Bed Thrust Bearing. *Proc. Inst. Mech. Eng. Part J J. Eng. Tribol.* **2020**, *234*, 134–144. [CrossRef]
19. Jang, G.H.; Lee, S.H.; Kim, H.W. Finite Element Analysis of the Coupled Journal and Thrust Bearing in a Computer Hard Disk Drive. *J. Tribol.* **2006**, *128*, 335–340. [CrossRef]

Disclaimer/Publisher's Note: The statements, opinions and data contained in all publications are solely those of the individual author(s) and contributor(s) and not of MDPI and/or the editor(s). MDPI and/or the editor(s) disclaim responsibility for any injury to people or property resulting from any ideas, methods, instructions or products referred to in the content.